UNSATURATED SOIL-RETAINING WALL INTERACTION: EXPERIMENTS AND THEORETICAL MODELLING

Thanh Vo and Adrian R. Russell
Centre for Infrastructure Engineering and Safety, School of Civil and Environmental Engineering, The University of New South Wales, Sydney, NSW, Australia, 2052

ABSTRACT

In this paper experimental observations and theoretical modelling outcomes are presented which show the significant effect suction has on the interaction between unsaturated soils and retaining walls. Firstly, a new testing facility and set of procedures for performing retaining wall model tests in unsaturated soils are described. The facility enables a rigid model wall to be rotated into or away from a soil sample about its toe. Results for samples of unsaturated decomposed granite are presented. Suction changes were measured using vibrating wire piezometers. Pressures on the wall were measured by earth pressure cells embedded in the wall face. Integrating the earth pressure profile enabled an equivalent load acting on the wall to be calculated, and was in reasonable agreement with the measured applied load. Soil deformations were recorded using particle image velocimetry. The pattern of soil deformation observed, particularly strain localisations, was similar to those in tests on dry sands. The suction increases measured during the test were consistent the volumetric dilation that occurred in the sample. Secondly, an extension of slip line theory to unsaturated soils is presented and applied to the rigid retaining wall problem. Suction is introduced using the effective stress concept. The predicted effective normal stresses were found to be in reasonable agreement with experimentally measured values.

1. INTRODUCTION

Retaining walls are ubiquitous to geotechnical engineering. Current design tools, which are concerned mainly with the lateral pressures retained soils exert on walls, were developed for cases when the retained soils are fully saturated or completely dry. In this paper, a new experimental testing facility to study the interaction between retaining walls and unsaturated soils is presented. The main design features are outlined including mechanisms enabling wall rotation at different points along the wall length, embedded earth pressure cells along the wall face enabling pressure profile to be established at different wall rotations, and the load application system enabling the moment about the rotation point to be recorded. The paper also discusses the sample preparation method adopted for a decomposed granite (sand-silt-clay mixture), the measurement of soil deformations using particle image velocimetry (PIV) [1] and suction using vibrating wire piezometers. Thus the facility is suited to fast testing in which sample moisture content remains constant while volumetric strain occurs and suction varies. Secondly, slip line theory is extended to the case where soil is unsaturated and used to analyse the retaining wall problem. Suction is introduced into soil strength and stress state using the effective stress concept [2] and an expression for the effective stress parameter [3]. The soil is assumed to obey the Mohr–Coulomb failure criterion and static equilibrium condition. Finally, the paper details a single experimental test result to highlight how extensive soil straining, dilation, suction, load, earth pressure and mode of deformation are interrelated and how they can be studied experimentally. Slip line theory predictions of earth pressures are, on average, in agreement with the experimentally measured values.

2. A NEW TESTING FACILITY

2.1 THE LATERAL EARTH PRESSURE RIG

The testing facility includes a lateral earth pressure (LEP) rig, specially designed and manufactured at The University of New South Wales. The LEP rig comprises a rigid steel plate (the retaining wall) embedded in a 0.6 m soil sample contained by a steel-framed box (Figure 1). The wall is 0.9 m long, 0.66 m wide and 40 mm thick, and hinged by two steel pins.

Six earth pressure cells are embedded into the wall face. Each cell has a diameter of 64 mm and a total thickness of 11 mm. The steel-framed box in which the steel plate rotates is 2.07 m long, 1.14 m high and 0.687 m wide. The ratio of tank length to retaining wall height is 2.3, which is generally sufficient to permit full development of passive wedges when the wall is rotated into the soil. One side is made of three acrylic panels 10 mm thick to enable visual observation and PIV data collection (Figure 1). An electric motor-driven screw jack, connected to a 45 kN capacity universal flat load cell, pushes or pulls the top of the wall and reacts against a square hollow steel bar bridging across the top of the box. Thus the steel plate may be rotated in either direction about the toe

(i.e. the pin in Figure 1). Displacements of the top of the steel plate are measured by two linear strain conversion transducers.

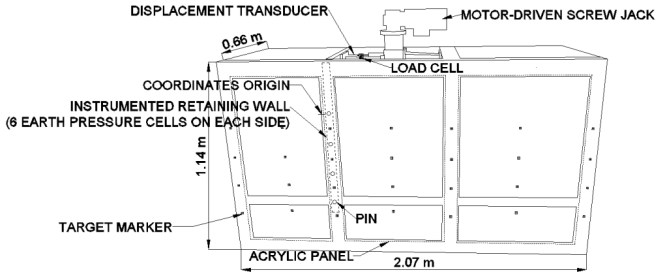

Figure 1: Lateral earth pressure rig details

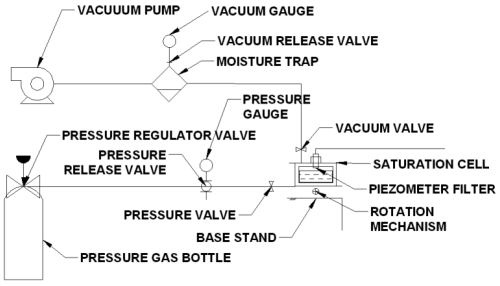

Figure 2: Vibrating wire piezometer saturation system

2.2 VIBRATING WIRE PIEZOMETERS, SATURATION SYSTEM AND PROCEDURE

The vibrating wire piezometers used are model PWS500 from Roctest. Their response to suction depends mainly on how well their tips, including both the high air entry ceramic and piezometer cavity, are saturated. A laboratory system similar to that of Take and Bolton [4] was set up to saturate the piezometer tips. It consisted of a saturation cell connected to a pressurised gas bottle and a rotary vacuum pump (Figure 2).

The step-by-step procedure used to saturate a piezometer tip involved initially separating the tip from the piezometer body, thoroughly cleaning and then drying the tips and body in an oven at 50 °C. The saturation cell was half-filled with de-aired water. The ceramic tip was then fastened to the piezometer body and then positioned in the saturation cell while orientated so that it was above the de-aired water line. An increasing vacuum was applied to the cell while the water surface always remained below the piezometer. When the piezometer reading indicated that a vacuum had been attained (a vacuum of 97 kPa was found to be sufficient corresponding to an absolute pressure of about 3 kPa), the cell was rotated 90° to submerge the piezometer in the de-aired water. De-aired water then flowed through the ceramic tip into the cavity behind. Then the vacuum valve was closed and the gas valve was opened (Figure 2). Gas pressure in the cell was slowly increased up to 450 kPa above atmosphere (about 550 kPa absolute) which was the maximum of the rated range of the piezometers. The piezometer was left in this state for 24 hours and resulted in sufficient saturation and response time to suction changes.

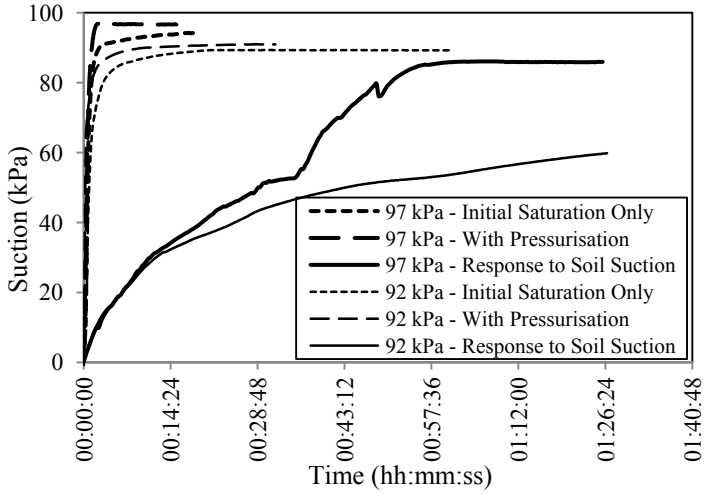

Figure 3: Responses of a piezometer to applied suction after saturation at 92 kPa and 97 kPa in the initial stage

Shown in Figure 3 are piezometer responses to suction after saturation at 92 kPa and 97 kPa in the initial stage, and with and without the subsequent application of an elevated pressure held constant for 24 hours. It is seen that a quicker response was obtained when the piezometer had initially been saturated at higher suction (97 kPa) and subsequently pressurised for 24 hours. It is also shown in Figure 3 that, once a piezometer has been saturated using a 97 kPa vacuum and subsequently pressurised, its response to an applied suction by either coming into contact with an unsaturated soil or applying a vacuum are rather different. It took less than 15 minutes to register the suction applied by a vacuum but up to one hour to register a similar suction applied by

coming into contact with an unsaturated soil. This may be due to reduced contact area between the surrounding pore water and the saturated ceramic tip or excess moisture on the tip [5].

Prior to embedment in the test soil, a saturated piezometer tip was covered by a thin layer of kaolin wetted at its liquid limit. This was done to slow down air diffusion through the tip and was found to be effective. In a trial, after having embedded a piezometer in an unsaturated soil with a suction of about 30 kPa for two months, the kaolin layer was still moist and the piezometer still responded well to suction changes.

3. TEST MATERIALS AND PROCEDURES

3.1 TEST MATERIALS

The test soil is decomposed granite taken from the catchment area of Lyell Dam, NSW. It is classified as silty sand, is well graded, and has a specific gravity of 2.55. Prior to testing the soil was passed through a 4.75 mm sieve to remove foreign debris (roots, sticks etc.), dried in oven and stored in sealed drums.

3.2 SOIL COMPACTION

When several thin soil layers are compacted on top of each other to form a sample, certain measures are needed to ensure uniformity of the compacted density throughout the sample. During compaction energy is transmitted from the compaction device through the layer being compacted to the underlying layers causing them to become denser. A number of procedures have been used to account for this and achieve equal densities in each layer. A similar approach to that of Bradshaw and Baxter [6] was adopted in this investigation. As an electric Kango percussion hammer fitted with a 180 mm square steel pad (rather than hand operated drop hammer) was used to apply the compaction energy, carefully controlling and varying the duration of compaction enabled the overall compaction energy put in to each layer to be constant.

A calibration procedure was initially carried out to determine how the compacting duration related to wet density for a single 90 mm layer. A linear relationship was observed between wet density and the logarithm of compaction duration, and that for a moisture content of 4.5 % and a wet density between 1700 kg/m^3 and 1850 kg/m^3, it can be expressed as:

$$\rho_w = 63.373 \ln(t) + 1593.1 \qquad \text{Eq. 1}$$

where $\rho_w \equiv$ wet density (kg/m^3) and $t \equiv$ compaction duration (s). Subsequent compaction trials enabled the computation of compaction times in each layer so that the effect of increasing density with depth can be accounted for and uniform layer densities were achieved (Vo and Russell [7]).

The soil sample in the testing rig was made up of ten 90 mm thick layers. First dry soil was mixed with water at the target moisture content in a drum mixer. The moist soil was bagged in 20 kg portions and cured for several weeks. Prior to placing a new layer, the surface was thoroughly scarified to about 10 mm depth. While soils were being compacted, the retaining wall was fixed in the vertical position.

3.3 DISPLACEMENT MEASUREMENT BY PIV

The PIV technique, also known as the digital image correlation technique, has been used by researchers to study movements of soil grains [1, 8-11]. A CANON Powershot G7 digital still camera with remote shooting capability was used. The captured images were each 3113 pixels by 1864 pixels in resolution. Setting up a PIV measuring exercise requires placing fixed target markers on the acrylic panels. The markers aid the matching of points in digital images to the physical test. They also enable correction of the systematic differences between the physical coordinates system containing the test rig and the image coordinate system. In this investigation 20 target markers were used, each taking up about 35 pixels by 35 pixels in an image, placed in a grid pattern shown in Figure 1. The physical coordinates of the target markers were measured relative to the origin. During the experiments natural light was prevented from entering the room. Artificial lighting was provided by two halogen lamps. This was to prevent any drastic change in image quality due to variation in natural light. Even so, it was found that background reflection on the acrylic panels was problematic, and a balance had to be struck between background reflection (due to low light) and an excess of light causing fixed 'washed-out' regions on the images. Since the patch size, patch spacing and search zone dimension need to be defined in using the PIV technique, an exercise was conducted to determine a suitable combination of these parameters for the rig setup. It was found that a patch size of 64 pixels by 64 pixels, a spacing interval of 32 pixels and search zone of 16 pixels resulted in a reasonable level of detail. The subsequent data interpretations produced very few wild displacement vectors.

3.4 TEST PROCEDURES

A result of a single test is outlined in section 6.1 in this paper. For this test, the soil was compacted at a moisture content of 0.045 and a void ratio of 0.54.

Four piezometers were embedded at four different depths: 0.18 m, 0.23 m, 0.32 m and 0.44 m. Three were placed close to the retaining wall (180 mm from the wall face) and one (the piezometer at 0.23 m depth) was placed further from the wall (590 mm from the wall face). The suctions measured by four piezometers prior to the test ranged from 55.5 kPa to 59.4 kPa with an average of 57.1 kPa.

After the final layer of soil was compacted, the soil surface was covered with plastic sheets to prevent moisture loss from exposure to air. The retaining wall was then rotated at a rate of 0.0106 degrees per minute. The total test duration was about 11 hours which was considered to be sufficiently long for piezometers to register fully the changes in suction but sufficiently short to assume a constant moisture content condition throughout the test soil. At the end of the test the wall had rotated to an angle ω of 6.94°.

4. AN EXTENSION TO THE SLIP LINE THEORY

4.1 LIMIT EQUILIBRIUM METHODS AND SLIP LINE THEORY

Earth pressure problems for saturated or dry soils are usually analysed by limit equilibrium methods [12-14] and the slip line theory [15-17]. In the limit equilibrium approach, soil is treated as a rigid material and divided into blocks. Force and moment equilibrium equations are used to find the failure surface corresponding to the lowest factor of safety. On the other hand, slip line theory treats soil as a continuous body. A failure criterion is combined with the condition of stress equilibrium to form the governing equations for this limiting state. While the slip line theory is more restricted than the limit equilibrium methods in terms of geometries and boundary conditions, it is more amenable to realistic soil behaviours [18-20] and solutions of simple problems can be found in closed form.

4.2 ASSUMPTIONS IN THE SLIP LINE THEORY

The standard assumptions in the slip line theory include Mohr–Coulomb failure criterion for soil and for interface, and the soil body satisfying static equilibrium condition. There are many possible extensions to these standard assumptions such as varying friction angle and varying ratio of volumetric strain increment to shear strain increment [21-24]. However, these extensions are usually specific to a soil type and significantly complicate analyses so the standard assumptions of soil obey the Mohr-Coulomb failure criterion and static equilibrium condition are adopted here.

4.3 THE EFFECTIVE STRESS CONCEPT

Informed by experimental evidence, Bishop [2] extended Terzaghi's effective stress to unsaturated soils:

$$\sigma' = \sigma + \chi s \qquad \text{Eq. 2}$$

where $\chi \equiv$ effective stress parameter, $s = (u_a - u_w) \equiv$ soil suction, $u_a \equiv$ pore air pressure and $u_a \equiv$ pore water pressure. Similar expressions have been adopted by others [25-27]. The effective stress parameter is influenced by many factors such as soil type, whether the soil is undergoing a drying or wetting cycle, the loading history leading to a particular value of degree of saturation [28] and particular soil structure [29]. Many expressions have been proposed for estimating the effective stress parameter. One of the most appealing is that proposed by Khalili and Khabbaz [3]:

$$\begin{cases} \chi = (s/s_e)^{-0.55}, s \geq s_e \\ \chi = 1\,, s < s_e \end{cases} \qquad \text{Eq. 3}$$

where $s_e \equiv$ suction value separating saturated from unsaturated states. Although χ in Eq. 3 contains no volumetric parameter, Eq. 3 and its variations [30, 31] were shown to be able to predict effective stress for a wide range of soils on both mechanical and hydraulic stress paths. One advantage of Eq. 3 is its simplicity. No more than the one parameter, i.e. the suction value separating saturated from unsaturated states, is required and it can be obtained in a soils laboratory.

4.4 GOVERNING EQUATIONS

With reference to the adopted coordinate system shown in Figure 4, the governing equations of the slip lines η and ξ can be derived from static equilibrium condition as:

$$\begin{cases} \mathrm{d}y/\mathrm{d}x = \tan(\theta + \mu_s) \\ \mathrm{d}\eta/\mathrm{d}x = \mathrm{C1}/\mathrm{C2} \end{cases} \quad \text{Eq. 4}$$

$$\begin{cases} \mathrm{d}y/\mathrm{d}x = \tan(\theta - \mu_s) \\ \mathrm{d}\xi/\mathrm{d}x = \mathrm{C3}/\mathrm{C4} \end{cases} \quad \text{Eq. 5}$$

where the terms $\mathrm{C1}, \mathrm{C2}, \mathrm{C3}$ and $\mathrm{C4}$ are given by:

$$\mathrm{C1} = -[\gamma_t + \partial(c'\cot\phi' + \chi s)/\partial x]\sin(\theta - \mu_s) + [\partial(c'\cot\phi' + \chi s)/\partial y]\cos(\theta - \mu_s)$$

$$\mathrm{C2} = 2\sigma'\sin\phi'\cos(\theta + \mu_s)$$

$$\mathrm{C3} = [\gamma_t + \partial(c'\cot\phi' + \chi s)/\partial x]\sin(\theta + \mu_s) - [\partial(c'\cot\phi' + \chi s)/\partial y]\cos(\theta + \mu_s)$$

$$\mathrm{C4} = 2\sigma'\sin\phi'\cos(\theta - \mu_s)$$

and the symbols μ_s, η, ξ are defined in the following expressions:

$$\mu_s = \pi/4 - \phi'/2 \quad \text{Eq. 6.1}$$

$$\eta = (1/2)\cot\phi'\ln(\sigma'/\sigma_0') + \theta \quad \text{Eq. 6.2}$$

$$\xi = (1/2)\cot\phi'\ln(\sigma'/\sigma_0') - \theta \quad \text{Eq. 6.3}$$

and $\sigma' = (\sigma_1' + \sigma_3')/2 \equiv$ effective mean stress, $\theta \equiv$ angle between the vertical axis and the major principal stress direction, $\gamma_t \equiv$ unit weight of the soil and $\sigma_0' \equiv$ a scaling stress.

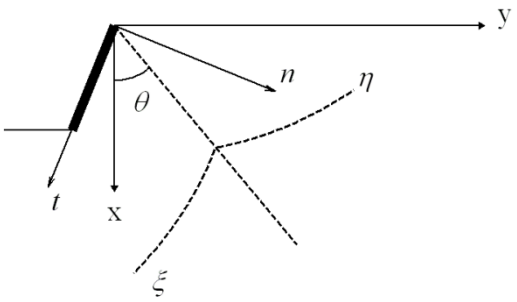

Figure 4: Adopted coordinates system and directions of slip lines

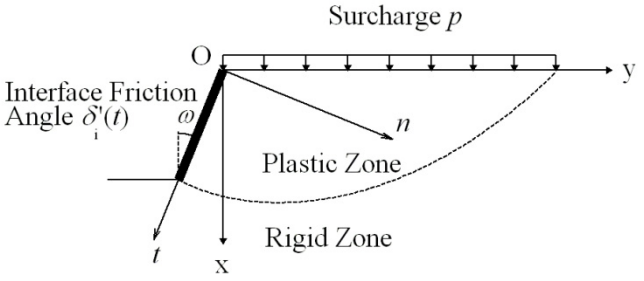

Figure 5: Conceptual model for the retaining wall–unsaturated soils interaction problem

Eq. 4 and Eq. 5 express two families of plane curves (η and ξ) and the relationships between the variables on each family. These curves are referred to as characteristic curves or simply slip lines in soil mechanics literature.

In solving boundary value problems, the above governing equations are usually discretised by the finite difference method. The finite difference expressions differ slightly depending on the location of the point being evaluated and the accuracy required. These expressions were detailed in Sokolovski [16] and Graham [32]. Similar numerical procedures were adopted in this investigation.

5. RETAINING WALL—UNSATURATED SOIL INTERACTION PROBLEM

5.1 CONCEPTUAL MODEL

The retaining wall–unsaturated soil interaction problem can be conceptually modelled by assuming a zone of soil next to an inclined wall (Figure 5) going into a state of limiting equilibrium (i.e. satisfying the Mohr-Coulomb failure criterion everywhere). The soil in this zone deforms plastically while the surrounding soil remains rigid. Another feature of this zone is that its lower boundary must pass through the base of the wall while the length of the soil surface boundary may vary. The surcharge p is assumed to be close to zero so the model approximates the free surcharge condition. The curves η and ξ are constructed based on this conceptual model and the stresses on the retaining wall (or anywhere in the plastic zone) can be obtained by integration along these η and ξ curves.

5.2 ADOPTED PARAMETERS

The adopted parameters for the conceptual model that are relevant to the experimental results presented in section 6.1 are listed in Table 1. A surcharge p of 1% of $\gamma_t L$ was adopted as it was shown by Graham [32] that this level of surcharge resulted in earth pressures sufficiently close to the free surcharge case. The soil friction angle ϕ' of 44° was selected and is significantly higher than the critical state friction angle (about 40° for this test material) due the low confining pressure considered in this problem. The soil suction value separating saturated from unsaturated states of 7.5 kPa was selected based on soil-water retention characteristics obtained from the results of mercury intrusion porosimetry tests.

Table 1: Adopted parameters for the theoretical model

	At $\omega = 1°$	At $\omega = 6.94°$
Surcharge p (% of $\gamma_t L$)	1%	1%
Length between soil surface and toe of wall L (m)	0.54	0.54
Wall inclination angle ω (°)	1	6.94
Soil cohesion c' (kPa)	0	0
Soil friction angle ϕ' (°)	44	44
Interface friction angle δ_i' (°)	22 at the top of wall and reduces linearly to 0 at toe of wall	22 at the top of wall and reduces linearly to 0 at toe of wall
Soil unit weight γ_t (kN/m^3)	17	17
Soil suction s (kPa)	57.1	57.1
Soil suction value separating saturated from unsaturated states s_e (kPa)	7.5	7.5
Interface suction value separating saturated from unsaturated states s_{ei} (kPa)	7.5	7.5

Retaining wall model testing carried out in dry soils showed that the interface friction angle was not constant along the wall and it strongly influenced the mobilised lateral earth pressures. The interface friction angle is dependent on the "normalised roughness" of the interface [33] and the relative density of the soil [34, 35].

For this conceptual model, an interface friction angle of 22° (i.e. half the soil friction) was assumed to be mobilised at the top of the wall and reduces linearly to 0° at the toe of the wall. The maximum interface friction angle of 22° was adopted because the retaining wall was relatively smooth and the test soil has a D_{50} value of 0.35 mm. The pattern of reducing interface friction with increasing depth was adopted as this was observed in many comparable model tests [36, 37].

6. EXPERIMENTAL RESULTS AND THEORETICAL MODELLING RESULTS

6.1 EXPERIMENTAL RESULTS

6.1.1 Lateral earth pressures and loads

The measured earth pressure profiles for three amounts of wall rotation (1°, 3° and 5°) are shown in Figure 6a. Consistent with observations made in dry sands [34, 35, 37], the earth pressures continuously changed as the wall rotated about its toe. The earth pressure near the top of the wall peaked first then gradually decreased with further wall rotation. Nearer the centre of the wall, the earth pressure peaked later then also decreased with further wall rotation. The earth pressure cell measurements were used to calculate an approximate equivalent load P that would be measured at the load cell. This was done by integrating the earth pressure profile. Taking moments about the centre of rotation P can be expressed as:

$$P = (2Nd - WH\sin\omega)/(2H\cos\omega) \qquad \text{Eq. 7}$$

where $N \equiv$ the normal load obtained by integrating the earth pressure profile (kN), $W \equiv$ the weight of the wall (kN), $H \equiv$ the distance between the centre of rotation and the load cell (m), $\omega \equiv$ the wall inclination angle and $d \equiv$ the distance between the centre of rotation and the centroid of the earth pressure profile (m).

This approximate equivalent load P is compared to the actual load P measured by the load cell in Figure 6b for different amounts of wall rotation. Although the loads were of similar magnitudes, different trends were observed. It is possible that the heavy fracturing of the upper portion of the soil sample caused stress localisations and unreliable earth pressures to be measured there. To account for this, the earth pressures measured by the top cell (closest to the surface) were replaced by linearly interpolated values (by depth) from

the pressures measured by the second cell. The resulting integrated load is plotted in Figure 6b as 'adjusted *P*'. The adjusted load shows closer agreement with load cell measurement compared to the unadjusted value.

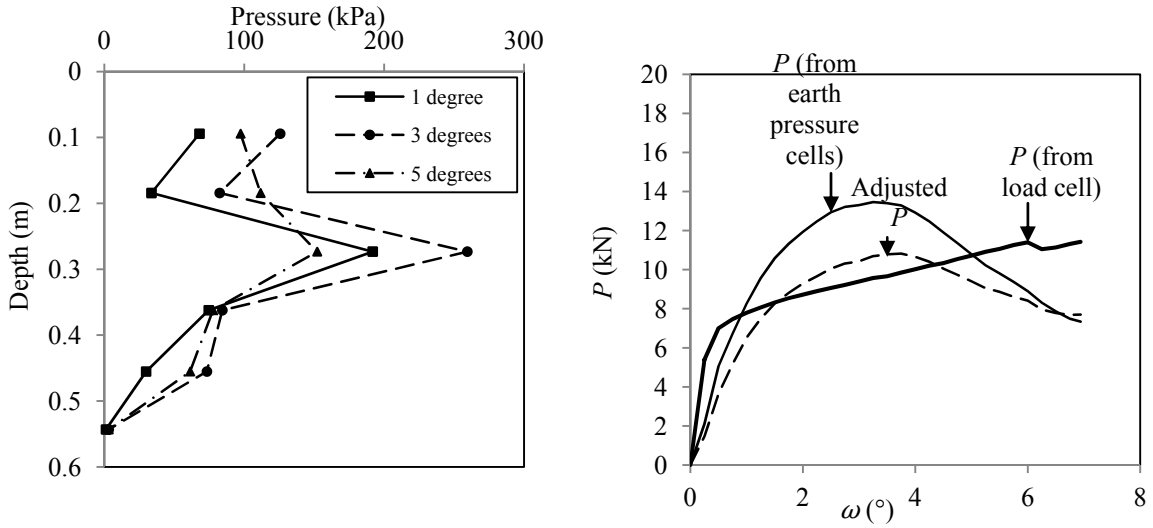

a. Measured earth pressures (in total stress)

b. Comparison of loads measured by earth pressure cells and by load cell

Figure 6: Experimental measurements of earth pressures and loads

6.1.2 Displacements and strain localisations

The displacement fields in the image coordinates system were computed and converted to their equivalents in the physical coordinates system using the GeoPIV software. The strain calculation program in the software was employed to calculate the total maximum shear strain γ between the wall rotations of 0° and 6.94°. It was observed that shear strains became significantly localized as rotation occurred. At the wall rotation angle of 0.5°, a distinct narrow band with high shear strain had formed near the top of the soil. As the wall rotated further, larger shear bands formed and cracks were observed. The cracks increased in extent with wall rotation; however, they almost exclusively located in the upper half of the sample near where the wall displacement was largest. This shear band pattern is shown in Figure 7 (the shaded area) for the rotation of 6.94°. Visible cracks are also shown in this figure as bold black lines.

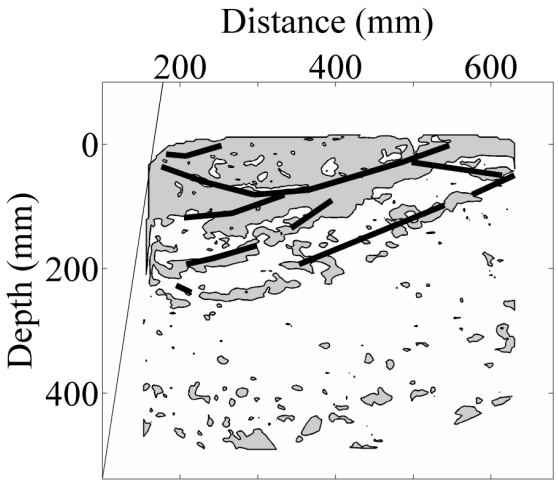

Figure 7: Regions with shear strain greater than 0.3 and observed cracks at 6.94 degrees (depth and distance are relative to the origin of the physical coordinates system shown in Figure 1)

6.1.3 Dilatancy and soil suction

The digital image of the strain field was divided into 4022 PIV patches, each being is 64 pixels by 64 pixels in size. To study the dilatancy of the test soil, the volumetric strains in the patches were calculated. For the patches corresponding to the regions containing two of the vibrating wire piezometers (those at 0.18 m and 0.32 m

depths), the average of the volumetric strain calculations was determined between the wall rotations of 0° and 6.94°. Each region was made up of a number of PIV patches so that four region sizes (50 mm by 50 mm, 100 mm by 100 mm, 150 mm by 150 mm and 200 mm by 200 mm) could be analysed and their results are shown in Figure 8a. Similar analyses were not conducted for the other two piezometers (at 0.23 m and 0.44 m depths) because their positions were outside the PIV mesh and very low suction changes were measured there.

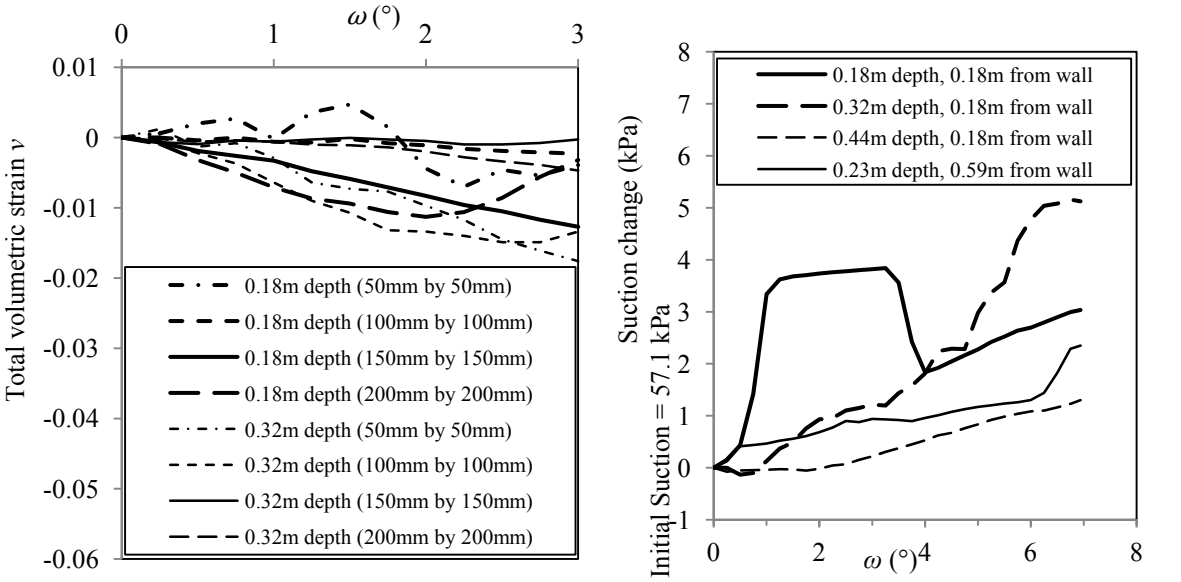

a. Inferred average volumetric strains at locations of vibrating wire piezometers

b. Suction changes measured by vibrating wire piezometers

Figure 8: Inferred volumetric strains at locations of piezometers and measured suctions

When moisture content is constant in an unsaturated soil, soil suction increases in response to increases in the soil volume. The measured changes in suction are shown in Figure 8b and were rather small compared to the initial suction. They were, however, significant in comparison to the suction changes caused by instrument drift (± 0.1 kPa) measured when there was no wall rotation and the soil surface was covered. There was a sudden increase in the suction measured by the piezometer at 0.18 m at a ω between 0.5° and 1° and a sudden drop at a ω of 3.25°. In comparison to the other three piezometers, the piezometer at 0.18 m depth was closest to the shear bands. It is probable that the jump and the drop were related to cracks developing and closing in the vicinity of the piezometer, and the associated movement of the piezometer within the soil.

6.2 THEORETICAL MODELLING RESULTS

Because the measured suction changes were small (Figure 8b) compared to the initial suction, it is assumed that suction stayed constant (at 57.1 kPa) during the test for the purpose of calculating effective normal stresses by Eq. 2 and Eq. 3. Other parameters of the theoretical model are listed in Table 1.

The predictions of effective normal stresses on the wall are shown in Figure 9a for two wall rotations (1° and 6.94°). It is seen that the theoretical model slightly over-predicts the experimental measurements near the top and near the toe, and under-predicts them near the mid-length of the wall. This is a direct consequence of the heavy fracturing of the soil near the top and the very little straining of the soil near the toe of the wall (Figure 7). The heavy fracturing of the soil near the top also caused stress to localise and resulted in higher earth pressures being measured near mid-length of the wall than predicted.

Figure 9b shows that more accurate predictions of the earth pressures near the mid-length of the wall could be obtained if a constant soil–wall interface friction of 22° is adopted. This assumption, however, resulted in poorer predictions of the earth pressures mobilised near the toe of the wall.

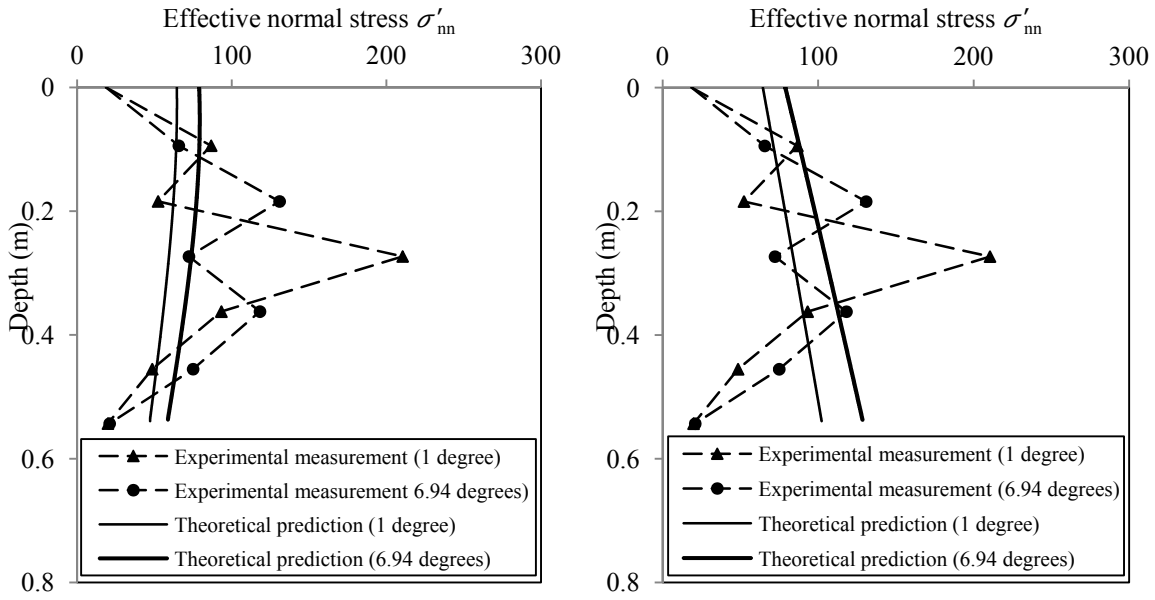

a. Theoretical predictions assuming varying soil–wall interface friction (Table 1)

b. Theoretical predictions assuming a constant soil–wall interface friction of 22°

Figure 9: Comparison between experimental measurements and theoretical predictions of earth pressures

7. CONCLUSIONS

A new experimental testing facility and testing procedures for carrying out retaining wall model tests in unsaturated soils have been presented. It was shown that commercially available vibrating wire piezometers could be saturated using a simple procedure to give reliable suction measurements during a test. Also, a hand-held electric percussive hammer was used to prepare a large soil sample at targeted moisture content and void ratio. Knowing how compaction energy was shared amongst soil layers enabled the control of energy input to achieve a uniform sample density. The hammer calibration and soil compaction procedures are readily adaptable to similar equipments and soils. The result of a single retaining wall model test was also presented in this paper. The patterns of stresses and strains developed were similar to those in tests conducted in dry sand. The total earth pressures varied as the wall rotated about its toe. The earth pressures measured near the top of the wall increased, peaked then decreased. It was shown that PIV may be used for strain analysis in retaining wall model tests in unsaturated soils. Analyses of the volumetric strains at the embedded locations of the piezometers also showed a slightly dilative behaviour and this may be correlated to the slight increase in the suctions measured at these locations. An extension to the slip line theory to unsaturated soils has also been presented. It was shown that the retaining wall model test could be conceptually modelled as a boundary value problem. The predictions of effective normal stresses on the wall were on average in agreement with the experimental values.

8. REFERENCES

[1] White DJ, Take WA, Bolton MD. Soil deformation measurement using particle image velocimetry (PIV) and photogrammetry. Géotechnique. 2003;53(7):619-31.

[2] Bishop AW. The principle of effective stress. Tecknish Ukeblad. 1959;106:859-63.

[3] Khalili N, Khabbaz MH. A unique relationship for chi for the determination of the shear strength of unsaturated soils. Géotechnique. 1998;48(5):681-7.

[4] Take WA, Bolton MD. Tensiometer saturation and the reliable measurement of soil suction. Géotechnique. 2003;53(2):159-72.

[5] Ridley AM, Dineen K, Burland JB, Vaughan PR. Soil matrix suction some examples of its measurement and application in geotechnical engineering. Géotechnique. 2003;53(2):241-53.

[6] Bradshaw AS, Baxter CDP. Sample preparation of silts for liquefaction testing. Geotechnical Testing Journal. 2007;30(4):1-9.

[7] Vo T, Russell AR. Unsaturated soil interacting with a rotating model wall. International Journal of Physical Modelling in Geotechnics. 2013;13(2):63-78.

[8] White DJ, Bolton MD. Displacement and strain paths during plane strain model pile installation in sand. Géotechnique. 2004;54(6):375-97.

[9] DeJong JT, White DJ, Randolph MF. Microscale observation and modeling of soil-structure interface behavior using Particle Image Velocimetry. Soils and Foundations. 2006;46(1):15-28.
[10] Ni Q, Hird CC, Guymer I. Physical modelling of pile penetration in clay using transparent soil and particle image velocimetry. Géotechnique. 2010;60(2):121-32.
[11] Niedostatkiewicz M, Lesniewska D, Tejchman J. Experimental analysis of shear zone patterns in cohesionless for earth pressure problems psing particle image velocimetry. Strain. 2010;47(s2):218-31.
[12] Coulomb CA. Essai sur une application des règles des maximis et minimis à quelques problèmes de statique relatifs à l'architecture. Mémoires de Mathématique et de Physique, Paris, 1773. 1776;7:343-82.
[13] Ohde J. Zur theorie des erddruckes unter besonderer berücksichtigung der erddruckverteilung. Die Bautechnik. 1938;16.
[14] Terzaghi K. Theoretical Soil Mechanics. New York: John Wiley and Sons, 1943.
[15] Shield RT. Stress and velocity fields in soil mechanics. Brown University, 1952.
[16] Sokolovski WV. Statics of Soil Media. 2nd ed. London: Butterworths, 1954.
[17] Rankine WJW. On the stability of loose earth. Philosophical Transactions of the Royal Society of London. 1857;47:9-27.
[18] Jenike AW, Shield RT. On the plastic flow of Coulomb solids beyond original failure. Journal of Applied Mechanics. 1959;81:599-602.
[19] Spencer AJM. A theory of the kinematics of ideal soils under plane strain conditions. Journal of the Mechanics and Physics of Solids. 1964;12:337-51.
[20] Jenike AW. Gravity flow of bulk solids.Bulletin of the Utah Engineering Experiment Station. Salt Lake City.1961.
[21] Serrano AA. Generalisation of the associated field method. The 5th European Conference on Soil Mechanics and Foundation Engineering. Madrid, Spain 1972. p. 355.
[22] Smith IAA. Stress and strain in a sand mass adjacent to a model wall (PhD thesis): Cambridge, UK, 1972.
[23] Atkinson JH, Potts DM. Calculation of stresses and deformations around shallow circular tunnels in soft ground by the method of associated fields. Conference on Computer Methods in Tunnel Design: The Institution of Civil Engineers, 1978. p. 61-84.
[24] Atkinson JH, Potts DM. A note on associated field solutions for boundary value problems in a variable p-variable v soil. Géotechnique. 1975;25(2):379-84.
[25] Jennings JE. A revised effective stress law for use in the prediction of the behaviour of unsaturated soils. Proceedings of Conference on Pore Pressure and Suction in Soils. London, UK: Butterworth, 1960. p. 26-30.
[26] Aitchison GD. Relationships of moisture content and effective stress functions in unsaturated soils. Proceedings of Conference on Pore Pressure and Suction in Soils. London: Butterworth, 1960. p. 47-52.
[27] Croney D, Coleman, Black WPM. The movement and distribution of water in soil in relation to highway design and performance.Highway Research Board Special Report No 40. Washington, D. C.1958.
[28] Bishop AW, Henkel DJ. The measurement of soil properties in the triaxial test. London, UK: Edward Arnold, 1957.
[29] Coleman JD. Stress-strain relations for partially saturated soils. Géotechnique. 1962;46(2):279-89.
[30] Khalili N. Effective stress in double porous media with two immiscible fluids. Geophysical Research Letters. 2005;32(15).
[31] Khalili N, Habte MA, Zargarbashi S. A fully coupled flow deformation model for cyclic analysis of unsaturated soils including hydraulic and mechanical hystereses. Computers and Geotechnics. 2008;35(6):872-89.
[32] Graham J. Calculation of passive pressure in sand. Canadian Geotechnical Journal. 1971;8(4):566-78.
[33] Kishida HU, M. Tests of the interface between sand and steel in the simple shear apparatus. Géotechnique. 1987;37(1).
[34] Rowe PW, Peaker K. Passive earth pressure measurements. Géotechnique. 1965;15(1):57-78.
[35] James RG, Bransby PL. Experimental and theoretical investigations of a passive earth pressure problem. Géotechnique. 1970;20(1):17-37.
[36] Bransby PL. Stress and strain in sand cause by rotation of a model wall (PhD thesis): Cambridge, UK, 1968.
[37] Bica AVD, Clayton CRI. An experimental study of the behaviour of embedded lengths of cantilever walls. Géotechnique. 1998;48(6):731.